ARTICLE

All optical switching of a single photon stream by excitonic depletion

Guillermo Muñoz-Matutano [1,2,3,7]*, Mattias Johnsson[1,2,7], Juan Martínez-Pastor[3], David Rivas Góngora[3,4], Luca Seravalli[5], Giovanna Trevisi[5], Paola Frigeri[5], Thomas Volz[1,2] & Massimo Gurioli[6]

Single semiconductor quantum dots have been extensively used to demonstrate the deterministic emission of high purity single photons. The single photon emission performance of these nanostructures has become very well controlled, offering high levels of photon indistinguishability and brightness. Ultimately, quantum technologies will require the development of a set of devices to manipulate and control the state of the photons. Here we measure and simulate a novel all-optical route to switch the single photon stream emitted from the excitonic transition in a single semiconductor quantum dot. A dual non-resonant excitation pumping scheme is used to engineer a switching device operated with GHz speeds, high differential contrasts, ultra-low power consumption and high single photon purity. Our device scheme can be replicated in many different zero dimensional semiconductors, providing a novel route towards developing a platform-independent on-chip design for high speed and low power consumption quantum devices.

[1] Department of Physics and Astronomy, Macquarie University, Sydney, NSW, Australia. [2] ARC Centre of Excellence for Engineered Quantum Systems, Macquarie University, Sydney, NSW 2109, Australia. [3] UMDO (Unidad Asociada al CSIC-IMM), Instituto de Ciencia de Materiales, Universidad de Valencia, P.O. Box 22085, 4607 Valencia, Spain. [4] Institute of Physics, Bijenička cesta 46, HR-10000 Zagreb, Croatia. [5] CNR-IMEM Institute, Parco delle Scienze 37a, I-43100 Parma, Italy. [6] Dipartimento di Fisica e Astronomia, LENS, Universita di Firenze, Via Sansone 1, I-50019 Firenze, Italy. [7] These authors contributed equally: Guillermo Muñoz-Matutano, Mattias Johnsson. *email: guillermo.munoz@uv.es

All-optical switchers or transistors are basic elements in the development of optical signal processing[1]. Nanoscale physical systems, which function as all-optical photonic devices, are receiving much attention due to their scalability and their quantum behaviour[2,3]. At present, there are many physical systems working as possible atomic and nanoscale all-optical logic devices, including trapped ions[4], single atoms[5], non-linear materials[6–8], single molecules[9], nitrogen vacancy centres in diamond[10], plasmonics devices[11] or exciton polaritons[12–14], among others. Due to their exceptionally high single-photon purity and indistinguishability[15,16], solutions where single semiconductor quantum dots (SQDs) act as the active material in the device deserve much of the attention[17]. All-optical logic operation with SQDs has been realized in quantum electrodynamics platforms, producing high-fidelity quantum controlled-NOT gates[18–20], single or few photon switchers[21,22] and all-photonic quantum repeaters[23]. A single SQD spin-to-single-photon switcher has been demonstrated in a nanobeam photonic waveguide platform[24], dipole–dipole interactions between QDs in a molecular configuration have been proposed to build an all-optical switcher[25] and two-colour laser excitation has demonstrated the switchability of the emitted photon statistics in colloidal QDs[26] and InAs QDs[27]. All of these efforts suggest new, near-future methods to implement all-in-one nanoscopic routes for developing photonic quantum technologies[28]. In this article we report the measurement and modelling of a new switching scheme to engineer a fast optical multiple state selector controlled by all-optical means and built on a simple and easy-to-replicate architecture. The development of such fast, low power, all-optical devices will aid the progress of near-future quantum photonic technologies[2,28,29].

Results

The physical mechanism of the switching is based on the carrier refilling process in a single SQD when the nanostructure is optically pumped in non-resonant dual-excitation conditions (see Fig. 1a): a continuous wave (cw) laser acts as the switcher input and a pulsed laser acts as the switcher control. When the control pulse arrives, the SQD undergoes a deviation from its steady-state carrier configuration, populating its higher order states and blocking the optical emission from low order states. The switcher output consists of a spectrally filtered single-photon stream from the low order SQD state recombination. The photon stream will be blocked when the control pulse arrives, and finally the emission from low order states will be recovered as the steady state is once again attained.

Switching by excitonic depletion. In single SQDs, the direct and exchange terms of the Coulomb interaction break the degeneracy of the neutral exciton (X^0), the positively and negatively charged exciton (the trions $X^{\pm 1}$) and biexciton (XX^0) states, producing four independent optical recombination channels. However all these states are connected through multiple carrier capture and escape dynamical processes (see Fig. 1b). For example, the carrier capture by a SQD containing a neutral exciton creates a charged exciton. This represents a quenching mechanism for the neutral exciton recombination. Similarly, the carrier capture by a SQD containing a charged exciton produces a biexciton. In these examples, the simple excitonic state depletion is related to the carrier kinetics in the SQD. In a previous study we demonstrated how excitonic transitions in a single SQD coupled to a 2D carrier reservoir, driven by high-power non-resonant pulsed excitation, can manifest a double-peaked time transient[30]. The double-peaked shape can be understood as an effective modulation of the excitonic decay time. When a high-power single laser pulse

excites non-resonantly the sample, thus being absorbed within the GaAs barrier, the single excitonic SQD state is very rapidly populated by the corresponding capture processes. However, as the reservoir still contains an excess of carriers, any subsequent carrier capture will deplete the single exciton state. This double-peaked decay was reproduced by a master equation for microstates (MEM) model[30,31].

In Fig. 1c the orange lines show the output of the model for the time-dependent X^0 and XX^0 population probabilities in the case where the SQD is pumped with conventional high-power single-pulse excitation. We found that the first, rapid peak is related to the initial and subsequent state refilling from the reservoir dynamics (labelled as i), while the second peak is related to the intrinsic excitonic decay time when reservoir is not playing a role in the dynamics (labelled as ii). Figure 1b shows a 3×3 matrix representation of all possible SQD carrier configurations simulated by the model, when only electron and hole S-levels are considered. The matrix depicts the single electron, single hole and exciton capture and escape processes and the electron and hole recombination producing photon emission. A more complete description of the model, as well as details on the numerical simulation, can be found in the Supplementary Note 1.

In the present work we have used the same MEM model to simulate the excitonic population probability evolution with single-colour and two-colour dual-excitation conditions: non-resonant cw excitation and non-resonant pulsed excitation, where the cw and pulsed lasers can have the same or differing wavelengths (see Fig. 1d, e). Similar dual-excitation schemes have been used to propose the dynamical photon blockade[32], or to control the spontaneous emission in coupled cavity systems[33]. Here, an initial non-resonant cw excitation creates a steady-state population distribution within the microstate time ensemble, and a second pulsed excitation arriving at time $t = 0$ drives the system far from this steady-state equilibrium, and then relaxes back to the initial equilibrium over a sub-nanosecond time scale. An example of the model output of the probability population for both X^0 and XX^0 is shown as the blue shaded region in Fig. 1c. As the pulse arrives, X^0 population is driven up to the biexciton state and its occupation probability goes to zero, depleting its population to fill the XX^0 state. This excited state filling reaches the maximum population probability in sub-nanosecond time scale, typically tens of picoseconds. As the XX^0 state begins to depopulate by photon recombination, the X^0 state starts to recover its steady-state probability. The time needed to re-populate the X^0 state is predominantly affected by the reservoir decay time, which governs the carrier population that is available to be captured by the SQD[30]. This excitonic depletion mechanism is optimal for an initial cw pumped steady state close to its saturation threshold, which represents its brighter emission rate and therefore more interesting for quantum technologies applications[15].

Figure 1f shows the set-up used in the experiments. We used three different excitation schemes. For the standard and the preliminary μ-photoluminescence (μ-PL) analysis we used a cw diode laser at 790 nm. For the single-colour, dual-excitation scheme we used a cw diode laser (Laser 1) and a pulsed laser diode operating at 40 MHz (Laser 2), both emitting at 790 nm. For the two-colour, dual-excitation scheme we used a cw diode laser (Laser 1) emitting at 830 nm and a pulsed laser diode emitting at 790 nm operating at 40 MHz (Laser 2). All these excitations conditions represent different variations of non-resonant optical pumping (see Fig. 1c). A fibre coupler was used to mix both laser sources and a fibre loop was used to produce a relative delay between pulses. The laser beam is coupled to an optical fibre and carried to the excitation arm of a diffraction-limited confocal microscope, working at liquid helium
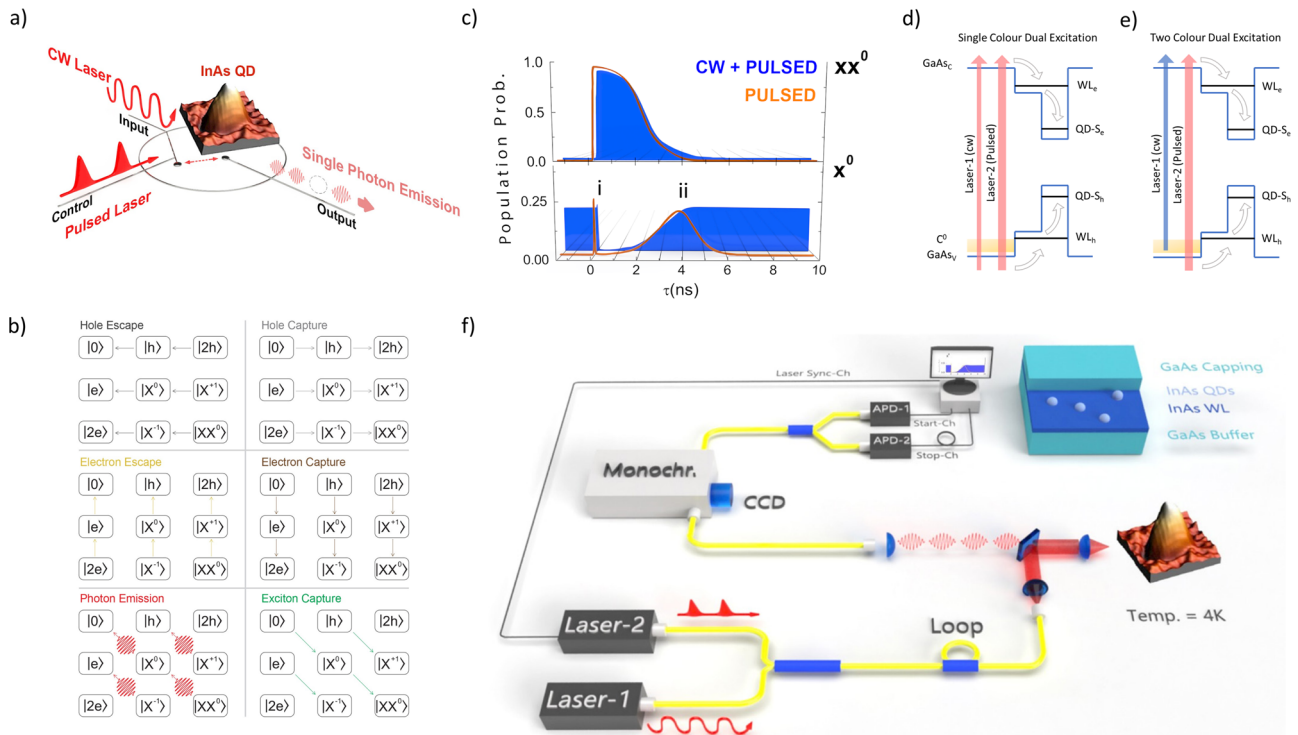
Fig. 1 Operation and fundamentals of the switching device. a An incoming continuous wave (cw) laser (Input) excites a single quantum dot. A second pulsed laser controls the switching gate. When the pulse arrives at the sample, all quantum dot simple excitonic transitions are blocked. The switcher output consists of an antibunched train of single photons, modulated by the control pulse sequence. **b** 3×3 matrix representing all quantum dot microstates considered in our model: vacuum state $|0\rangle$, single electron ($|e\rangle$) and single hole $|h\rangle$ states, two electron $|2e\rangle$ and two hole $|2h\rangle$ states, neutral exciton $|x^0\rangle$ and both negative $|X^{-1}\rangle$ and positive trions $|X^{+1}\rangle$ and neutral biexciton $|XX^0\rangle$. Vertical lines represent single electron capture (downwards) and escape (upwards), while horizontal lines represent single hole capture (rightwards) and escape (leftwards). Downward diagonal lines represent the capture of a single exciton, and upwards curly diagonal arrows represent single-photon emission. **c** Model simulation example of the neutral exciton (X^0) and biexciton population (XX^0) probability evolution in time as the system is pumped with single-pulsed excitation (orange lines) and with dual excitation (bluish shadows). **d** Non-resonant pumping energy schemes for single-colour dual excitation (both cw and pulsed lasers are tuned to 790 nm). **e** Non-resonant pumping energy schemes for two-colour dual excitation (cw laser is tuned to 830 nm, resonant to the residual carbon impurities (C^0-e) transition, and the pulsed laser is tuned to 790 nm). The energy diagram corresponds to the GaAs conduction and valence band energies, the bidimensional carrier reservoir (WL) and the quantum dot S-level electron and hole energies. White arrows indicate the carrier relaxation path. **f** Set-up arrangement. One cw diode laser and a second pulsed laser are coupled to a single-mode fibre. A second fibre coupler is used to induce a relative separation between pulses. The signal from both lasers is directed to the excitation arm of a confocal microscope. Photon emission from a single InAs quantum dot is collected and coupled to a single-mode fibre, and directed to the spectrum recorder or to the time resolved single-photon counter analyser.

temperature (4 K). Light emitted from a single SQD was recorded in μ-PL, μ-Time Resolved Photoluminescence (μ-TRPL) and photon correlation experiments. Finally, Fig. 1f includes the schematics of the SQD sample epitaxy (in blue).

Single-colour switching. Figure 2a shows experimental μ-TRPL results of the X^0 optical transition when pumped under single-colour dual excitation (i.e. 790 nm excition for both the cw control field and the pulse). The pulsed laser power is increased from 10 to 125 nW from the bottom to the top, while within each panel the mean power of the cw laser is increased from 0 to 450 nW. The solid orange lines show the case corresponding to conventional X^0 μ-TRPL, i.e. with the cw laser turned off. The grey lines show dual-excitation X^0 μ-TRPL as a function of cw power. Finally, blue lines show the dual-excitation μ-TRPL case when the X^0 steady-state population is near saturation for cw laser mean power of 450 nW. Figure 2b shows population probability from the model simulation for the same pumping conditions, and are in excellent agreement with the experimental results. The entire μ-TRPL data set provides a detailed map of the X^0 optical time transients as a function of input and control lasers. As can be seen, the X^0 optical transition follows an optimal

on/off/on sequence (switching) when the cw laser provides a saturated steady-state population, and the control laser provides high-power pulses. This means that the average excitation power of the control laser can act as a switch controller. We can define the following two different excitation limits: (i) the SQD is driven by high-power cw laser and high-power pulsed laser (Fig. 2c), resulting in a functional switch. (ii) The SQD is driven by high-power cw laser and low-power pulsed laser (Fig. 2d), disabling the switching functionality. Figure 2c, d shows experimental measurement and model simulation for the enabled (i) and disabled (ii) switching states, defined by input mean cw power of 200 nW and mean control powers of (i) 125 nW and (ii) 10 nW.

Two-colour switching. It is noteworthy that our switching proposal is not restricted to only the XX^0 to X^0 cascade, but also works for any intermediate excitonic transition within a multi-excitonic cascade. This is the case for the negative or positive trion states (labelled as X^{-1} and X^{+1} in Fig. 1b). Trions, which consist of a three-particle configuration (two electrons and one hole, or two holes and one electron), can populate the XX^0 state via the capture of single carrier (single hole or single electron,
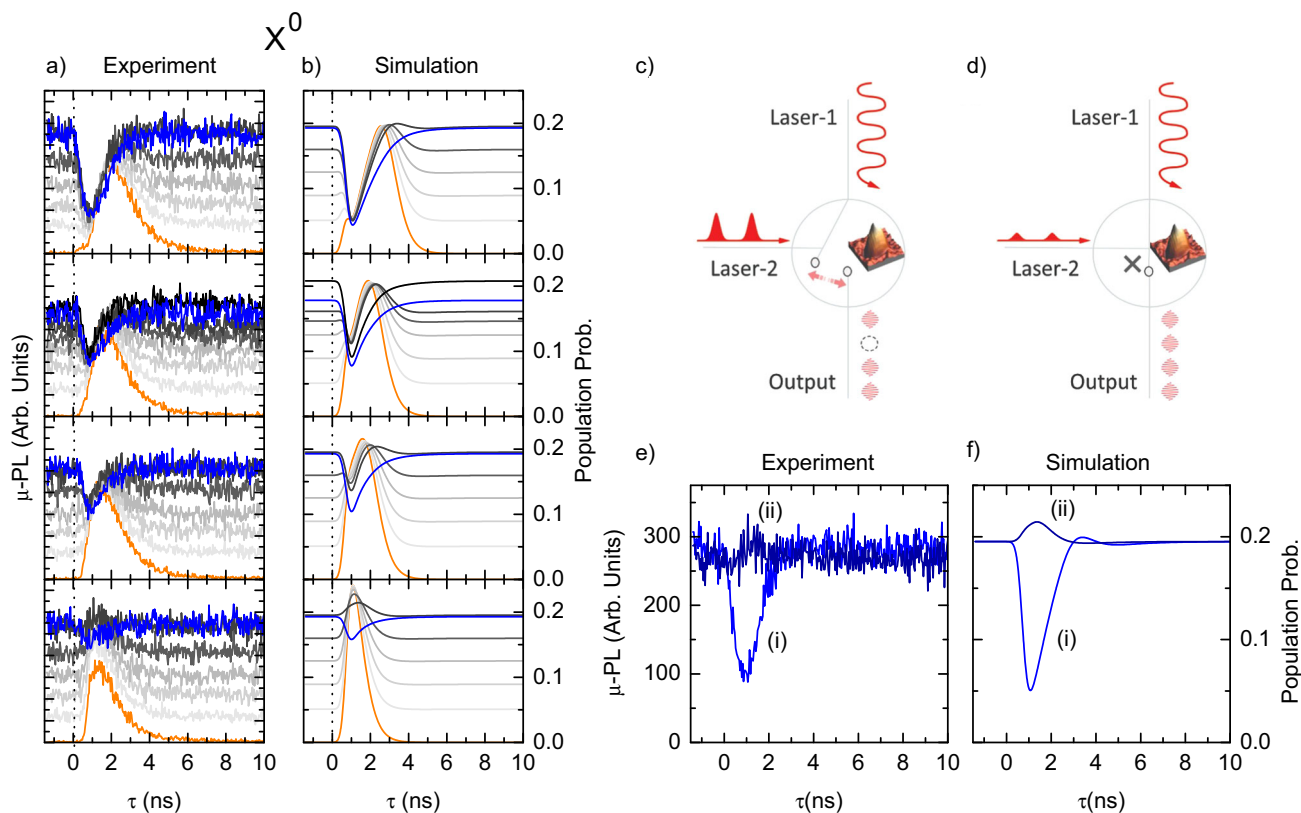
Fig. 2 X⁰ switching under single-colour dual excitation. a Experimental time resolved photoluminescence under combined 790 nm continuous wave (cw) and 790 nm pulsed laser excitation. In each panel the mean power of the cw laser is increased from 0 (orange lines) to 500 nW (blue lines). Intermediate cw laser powers (30, 60, 100, 140 and 200 nW) are represented with grey lines. The mean power of the pulsed laser increases from the bottom panels to the top panels, corresponding to 10, 33, 50 and 125 nW. **b** Population probability from the model simulation for the same pumping conditions. **c, d** Schematic representation of the single-colour, dual-excitation switching proposal with high and low pulsed laser power. **c** shows the situation where the switcher is operated in its enabled state, and **d** shows the situation where the switcher is in the disabled state. **e** Experimental time resolved photoluminescence measurements with the switcher enabled (i) (cw mean power = 200 nW and pulsed mean power = 125 nW) and disabled (ii) (cw mean power = 200 nW and pulsed mean power = 10 nW). **f** Model simulation for the same parameters in **e**.

respectively). This represents the unique refilling path connecting a higher configuration state described in our model framework. However, in a fully realistic model where P-levels of the SQDs are present, trions can be the feeding states for single charged biexcitons, or hot excitonic states[34].

In order to validate these assumptions, we studied the switching behaviour in a two-colour excitation scenario in a second SQD. In previous studies it was found that a laser wavelength tuned to the unintentional carbon impurities present in the molecular-beam epitaxy (MBE) growth (around 1.49 eV ~ 830 nm), enhances the negative trion relative optical intensity in the μ-PL spectrum[27,35]. Here, we take advantage of this excitation wavelength dependence of the trion relative intensity to study the switching behaviour when the cw input laser is tuned to 830 nm (Laser 1 in Fig. 3a). This two-colour excitation scheme provides an interesting advantage, as the fast switching can be accompanied by spectral isolation of the excitonic transitions. Figure 3b shows the μ-PL spectrum measurement when pumping with a pulsed 790 nm control laser (red line), with an 830 nm cw input laser (blue line), and with both input and control lasers (black line). As can be seen, the input cw laser enhances the X⁻¹ relative optical intensity, selecting that particular SQD spectral transition[35]. However, the pulsed control laser alone selects the XX⁰ to X⁰ cascade emission and the spectrum only shows this recombination path. Finally, when both lasers are switched on, both transitions are present. Figure 3c shows μ-TRPL transients

for the X⁻¹ and X⁰ transitions under the same excitation conditions shown in Fig. 3b. The bottom panel shows the X⁻¹ transient when pumping with the 830 cw laser (in blue) and the X⁰ transient when pumping with 790 pulsed laser (in red). The top panel shows both X⁻¹ (blue) and X⁰ (red) transients when pumping with both lasers. As can be seen, the switching is accompanied by a redistribution of the X⁻¹/X⁰ population probability ratio during the application of the pulsed laser. In Fig. 3d we have plotted the selective pumping efficiency[35] as a function of time, defined as $\Delta r(t) = \frac{I^{X^{-1}}(t) - I^{X^0}(t)}{I^{X^{-1}}(t) + I^{X^0}(t)}$. We have included blue and red shadows to highlight the regimes where X⁻¹ or X⁰ state recombination is dominant, respectively. Prior to the arrival of the pulse, the probability of each state is almost identical, meaning $\Delta r \sim 0$. However, when the 790 nm laser pulse arrives Δr becomes negative (approximately −0.53), indicating ~77%/23% probability for the X⁰/X⁻¹ transition. In this case, due to the long single-particle escape times (see Supplementary Table 1) present in the X⁻¹ to X⁰ state switching, the full equilibrium condition requires longer times compared with the single-colour case. However, it is possible to compensate for this reduction in switching speed by, for example, including Schottky diodes to produce a faster drain channel for single electrons/holes. We also note that the contrast shown in Fig. 3d is not optimal, as the pulse and cw laser power were chosen to return a spectral signal amplitude equal in magnitude for both X⁻¹ and X⁰
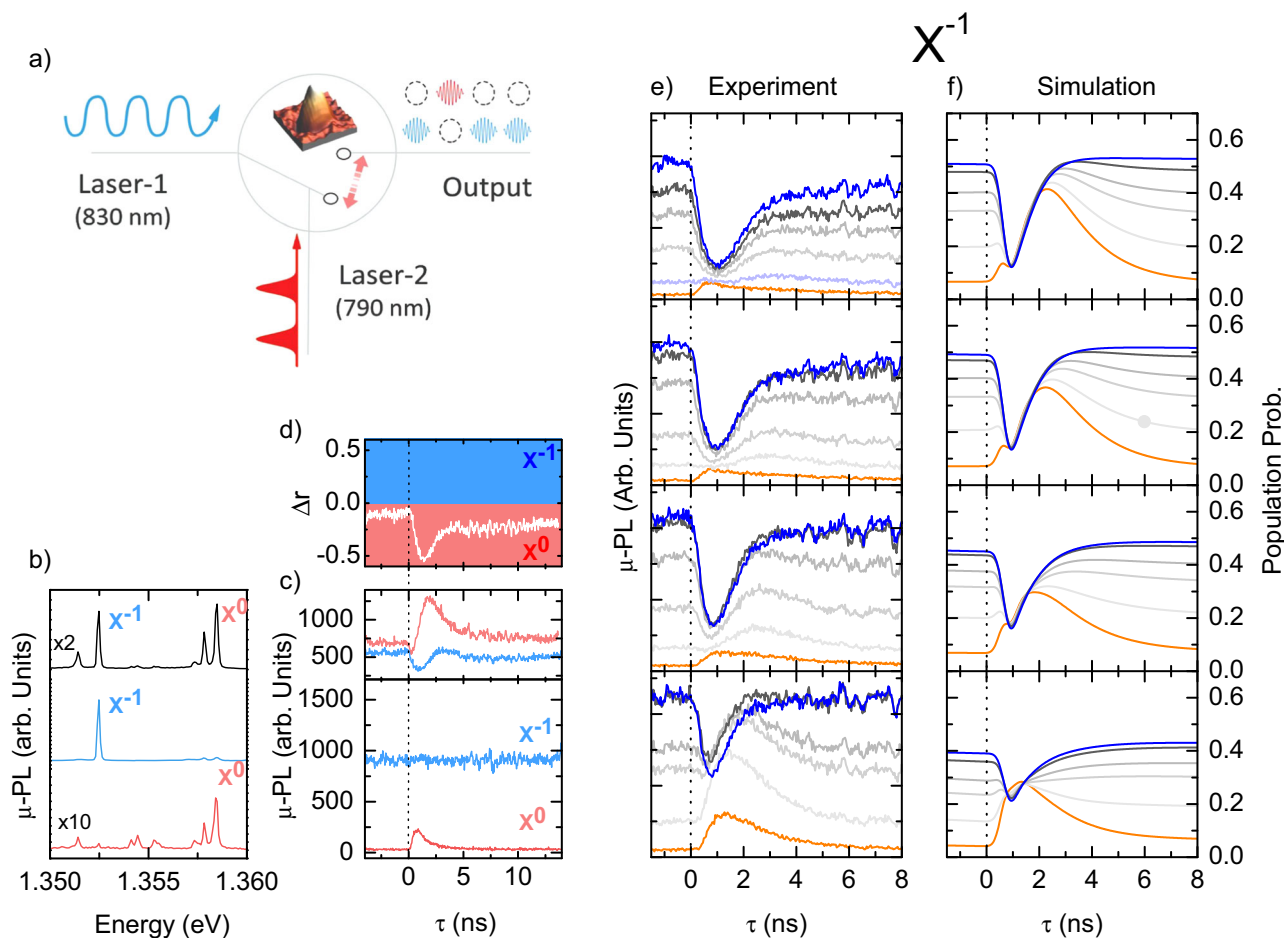
Fig. 3 X^{-1} switching under two-colour dual excitation. a Schematic representation of the two-colour dual-excitation switching proposal. Here the 830 nm continuous wave (cw) laser (Laser 1 shown in blue) is used as the switcher input channel and the 790 nm pulsed laser (Laser 2 in red) for the control, as before. **b** μ-Photoluminescence spectrum acquisition under 790 nm pulsed excitation (red line), under 830 nm cw excitation (blue line), and with both lasers (black line). **c** Time resolved photoluminescence with same excitation conditions in **b**, for the X^{-1} transition (in blue) and the X^0 transition (in red). **d** Evolution of the selective pumping efficiency (Δr) as a function of time. **e** Experimental time resolved photoluminescence under 830 nm cw and 790 nm pulsed laser excitation. cw laser mean power is increased from 10 μW (orange lines) to 300 μW (blue lines). Intermediate powers (40, 85, 120 and 190 μW) are represented with grey lines. The mean power of the pulsed laser increases from the bottom panels to the top panels, corresponding to 1, 3, 6 and 8.5 μW (top panels). **f** Model simulation for the same parameters in **e**.

transitions. As will be discussed below, the switching contrast can be modulated with the external laser pulse power.

Figure 3e shows the experimental μ-TRPL of the X^{-1} optical transition when the SQD is pumped with this two-colour dual-excitation scheme. Here mean pulse power is increased from 1 to 8.5 μW from bottom to top, while within each panel cw mean power is increased from 10 to 300 μW. Figure 3f shows population probability from the model simulation for the same pumping conditions. In order to provide the best match between the model simulation and experimental results, due to the significantly higher power excitation conditions used here, we included the effect of the power excitation dependence on the carrier diffusion length[36]. The switching of X^{-1} is clearly demonstrated and it agrees with the predicted trend by our MEM model as in our previous single-colour excitation. Nonetheless, for X^{-1} the quantitative agreement with the model is poorer than was the case for X^0, as the model approximations are less likely to be fulfilled for trions. As shown in Fig. 3f, our model gives an X^{-1} μ-TRPL amplitude higher than in the experiment (continuous orange lines). This is mainly due to restricting the model to S-levels of the SQDs, whereas more realistically the X^{-1} μ-TRPL amplitude is affected by the carrier

refilling of higher order states, which are not included in our simplified 3×3 microstate matrix. Despite these discrepancies, the simulations with the simple MEM model show a good qualitative agreement with the experiment, reproducing both the switching amplitude and its time scale.

Switching figures of merit. With the aim to extract a set of quantitative parameters, we have analysed the switching contrast and the switching speed for both SQDs, whose characteristics are shown in Figs. 2 and 3. Figure 4a shows the switching contrast for X^0 state under the single-colour dual-excitation experiment (SQD in Fig. 2). This parameter is defined as $(1 - \frac{A_L}{A_{SS}})$, where A_L is the integrated area around the lower value of the switch and A_{SS} is the integrated area around the steady-state population. Both areas are calculated with integration over the time response of the system (400 ps). We carried out this analysis for both the experimental measurements (solid dots), and for model simulations (straight lines). Figure 4b shows a similar analysis for the X^{-1} state under two-colour dual-excitation conditions (SQD in Fig. 3). As can be seen, there is excellent agreement between the experiment and the simulation, returning a maximum
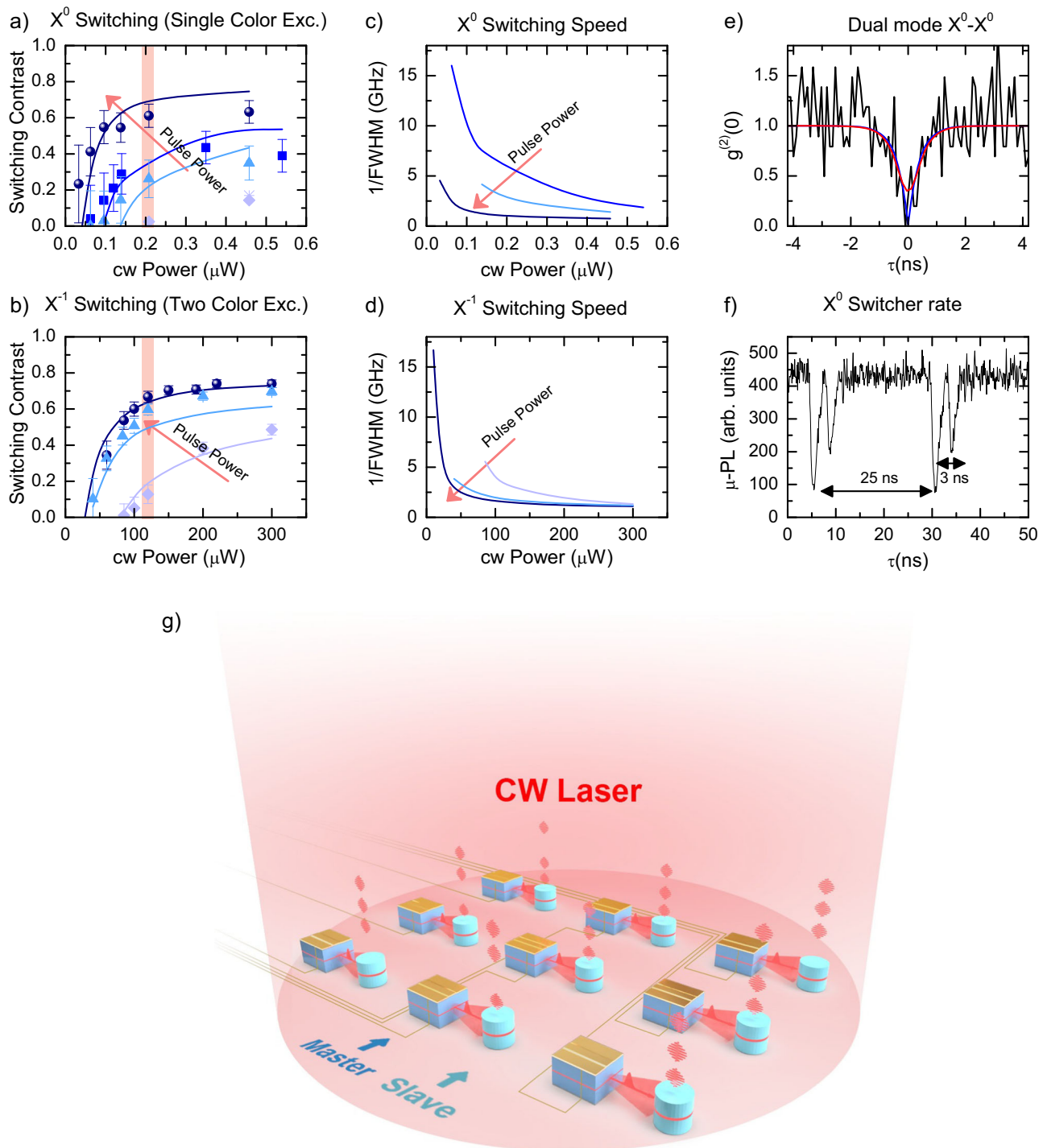
Fig. 4 Switching figures of merits and on-chip proposal. a Switching contrast as a function of continuous wave (cw) laser excitation mean power for the X^0 quantum dot transition under single-colour, dual-excitation conditions. Each colour corresponds to a different pulsed laser mean power (purple: 10 nW; light blue: 30 nW; blue: 50 nw; dark blue: 125 nW). **b** Switching contrast as a function of cw laser excitation mean power for the X^{-1} quantum dot transition under two-colour dual-excitation conditions. Each line corresponds to a different pulsed laser mean power (purple: 1 μW; light blue: 3 μW; dark blue: 8.5 μW). In both **a** and **b** scattered data and straight lines correspond to the experimental measurement and model simulation of the switching contrast, while red arrows indicate the direction corresponding to increased pulsed laser mean power, and the red shaded regions highlight the highest switching contrast between enabled and disabled switcher states. Vertical error bars are calculated assuming Poisson noise distribution in the integrated signal. **c**, **d** Switching speed for the X^0 and X^{-1} under single- and two-colour dual-excitation conditions, respectively. The switching speed is defined as the inverse of the full width at half maximum of the switch dip (1/FWHM), in frequency units. **e** X^0 photon autocorrelation under single-colour dual excitation operated with the highest switching contrast conditions (cw laser mean power = 200 nW, pulsed laser mean power = 125 nW). Red and blue lines correspond to the best fit to a two level model with and without the convolution with a Gaussian of FWHM 400 ps to include the effect of the system response. The fit returns $g^{(2)}(0) = 0.1 \pm 0.2$. **f** Evaluation of the switcher repetition rate, returning a rate of 300 MHZ. **g** Schematics of an array of switchers consisting of master and slave pairs. In this proposed device a cw input laser will drive the entire array, where each independent control laser (master diode) will enable or disable the switching mechanism of the optical emission of a single semiconductor quantum dot placed in the slave counterpart.

contrast when the cw laser pumps the excitonic transition (X^0 or X^{-1}) close to its saturation threshold (red shaded region; ~200 nW in Fig. 4a and 120 μW in Fig. 4b). In this situation, a high-power control pulse returns a switching contrast around 60%, while the low-power control returns a contrast less than 10%. If cw power is increased above the excitonic saturation threshold, the switching contrast with high-power control increases up to ~70%, however the relative contrast between both high and low control states is decreased, as the low-power pulse returns contrast around 20–40%.

We also examined the switching speed, defined as the inverse of the full width at half maximum (FWHM) of the switching dip (Fig. 4c, d). It is important to notice here that the value of the FWHM in time is calculated from the analysis of the model simulation output, before the convolution with the system response. This provides us an indirect estimation of the hidden but real physical speed of the device. Both the single- and two-colour excitation conditions show similar trends. As the control power increases, the switching speed decreases. Similarly, as cw input power increases, switching speed decreases. Although maximum speeds reach tens of GHz, operating the system under pumping conditions giving the maximum switching contrast yields a device speed of 1.0 and 1.2 GHz for the X^0 and X^{-1} states, respectively. Comparing our scheme of injecting carriers into the SQDs to those using electrical switching with gates, our approach is in general faster[37,38], and also could work for the X^0–XX^0 cascade, which is of great interest for the generation of entangled photon pairs[39].

Finally, we analysed both the single-photon purity and the switching repetition rate of the device. Figure 4e shows the measurement of the X^0 photon autocorrelation under single-colour dual excitation at the highest operational device performance (200 nW cw input power and 125 nW pulsed control power). Red and blue lines show the fit with a two level system model convoluted with and without a Gaussian function (FWHM ~ 400 ps), respectively. Our analysis returns $g^{(2)}(0) = 0.1 \pm 0.2$. We define the measurement error from the square root of the non-correlated coincidences (at delay time ≫ 0). The switching device shows a high single-photon purity emission, highly desirable for many realistic quantum technologies[15]. In order to quantify the switcher modulation capability, in Fig. 4f we measured the switching mechanism over a larger time span. We included an optical circulation loop within the excitation fibre (see Fig. 1d) in order to reduce the time delay between two consecutive pulses. As can be seen, we managed to reduce this delay to as little as 3 ns. The reduced amplitude of the second switch is due to the lower power contained in the looped pulse. Although this measurement provides an estimation of the switching modulation performance, easily working at 300 MHz, it does not represent an upper bound, which will be only limited by the steady-state recovery time of the excitonic transition and the specific SQD carrier dynamics. We conclude our device performance analysis with an estimate of the power required to switch a single bit. Assuming the control laser beam has 125 nW averaged power, each control pulse contains ~3 fJ. With a carrier diffusion length in the reservoir of ~100 nm[40] and a spot size of diameter ~1.2 μm we require ~0.08 fJ to trigger the switch. This important reduction in the device power consumption is mainly due to the SQD 0D density of states[17], as each excitonic microstate moves from absorption to transparency by the capture of single carriers.

Discussion
After the previous analysis, it is worth highlighting several general features of the device. Firstly, our proposal represents a nano-sized device, as typical QD dimensions lie in the 10–20 nm diameter range, and hence ideal to develop large, in-plane arrays of switchers, as we discuss below. Secondly, this device is operated at GHz speeds and tens of attowatt absorbed powers, which represents a good power/speed trade-off[17,41]. Also, although non-resonant excitation of a single SQD can reduce photon indistinguishability[15], in our scheme the non-resonant excitation provides a number of important features. Our device does not require critical biasing, meaning a single input laser can feed multiple single SQDs, without the need to critically tune the laser wavelength or power for each nanostructure[41]. Non-resonant excitation produces multiple single excitonic optical switches at different wavelengths, as for example from single excitons (X^0) or negative and positive trions (X^{-1} and X^{+1}). As we have described above, it is possible to modulate the relative X^{-1}/X^0 intensity emission by varying the input laser wavelength (Fig. 3b), which allows tunability of the wavelength multiplexed switching, and hence the incorporation of a fast exciton/trion optical state selector (see Fig. 3b, c)[35]. Another important advantage relies on the fundamental physical mechanism of the switching effect. As the fast carrier depletion arises from carrier refilling in a single SQD coupled to a reservoir and the subsequent modulation of the effective excitonic decay, we believe that the same switching feature will be found in many similar semiconductor nanostructures, such as colloidal core/shell SQDs[26], pre-patterned SQDs[42], droplet epitaxy QDs[43] or the newest quantum dots in 2D monolayer semiconductors[44,45], where spatially localized exciton and multiexciton transitions have recently been analysed[46]. At the same time we do not see any fundamental limitations in reproducing the same effect with SQDs emitting at longer wavelengths[47] or at higher temperatures[48], as in many of these nanostructures one finds biexcitonic/excitonic cascade emission with state saturation conditions and continuum reservoir states, where single-photon emission from single excitonic transition has been shown between 4 and 300 K[48]. Hence our proposed scheme represents a platform-independent design that can be implemented with many semiconductor 0D nanostructures. Furthermore, as this proposal does not need any external cavity engineering, it represents a robust design to reduce the device complexity and engineering costs.

Finally, we discuss a possible future implementation of our scheme that will allow more complex operations. From a techno-logical point of view, it is desirable to increase the device on-chip scalability. One step towards this goal is the implementation of an electrical integrated pumping scheme to independently drive and tune an array of optical cavities coupled to QDs. In order to avoid the issues arising from conventional electronic driving, the use of hybrid electric/optical pumping schemes has been proposed[49]. In these hybrid device schemes, slave QD epitaxies are usually pumped under non-resonant optical excitation from an electrically driven master diode grown in their vicinity. Our switching proposal can be adapted in similar master and slave partner epitaxies (Fig. 4g). A shared cw input laser (using a laser spot covering the entire array area) will act as a general input. However, each master diode will inject an independent control pulse that will deplete simple excitonic transitions only in its own slave counterpart. The end result is a device that creates an array of independent optical switchers of single-photon streams.

Although our method has many advantages, some aspects could be improved when considering future implementations. As our scheme uses non-resonant excitation, leading to the benefits described above, the output from an SQD will not match the input wavelength, meaning using the device in a cascadable manner is not trivial. Also, due to the non-resonant excitation, some reduction in the degree of photon indistinguishability can be expected[15]. However, both limitations would be mitigated if resonant excitation of the SQD microstates can produce similar power-dependent carrier depletion.

In summary, we have presented and explained a novel mechanism to build all-optical switchers using semiconductor single-photon emitters, which has been experimentally tested and can be well-reproduced theoretically by a MEM model. We have analysed the device performance as a function of multiple input and control parameters, obtaining sub-nanosecond switching times, low-power consumption, high switching contrast and high single-photon purity. Finally, we have demonstrated a number of interesting features of our device, and described possible future implementations for on-chip integration.

Methods

Photoluminescence and photon correlation experiments. An Andor technology CCD was attached at the monochromator front output in order to record the μ-PL spectra. μ-TRPL was obtained by filtering the μ-PL signal with a monochromator, and coupling the output signal to an avalanche photodiode (APD) through optical fibres. The pulsed laser trigger and the electrical APD output were directed to the sync and stop channels of a correlated single-photon counting card (TCSPC), respectively, (returning an experimental response ~400 ps). For the autocorrelation experiments we used a conventional Hanbury-Brown and Twiss scheme, with a fibre coupler acting as a beam splitter (50/50 for $\lambda = 980$ nm). Each fibre coupler output was directed to two APDs, both connected to the start and stop TCSPC card channels.

Sample growth. The SQDs were grown by MBE on a GaAs substrate, following Stranski–Krastanov growth. After a 100-nm-thick GaAs buffer, InAs has been deposited at a low growth rate (0.009 ML/s) at 535 °C with an equivalent coverage of 2.5 ML/s; the growth ended with a 100-nm-thick GaAs cap grown by atomic layer MBE at 360 °C[50]. During the InAs deposition, the substrate was not azimuthally rotated, thus obtaining a continuous variation of the InAs coverage throughout the sample surface[51]. These conditions resulted in a density of InAs QDs of about 16 QDs μm^{-2}, as estimated by atomic force microscopy (AFM) carried out on uncapped samples grown under the same conditions. Information about the AFM and ensemble photoluminescence characterization can be found elsewhere[40].

Data availability

The data that support the findings of this study are available from the corresponding author upon reasonable request.

References

1. Sasikala, V. & Chitra, K. All optical switching and associated technologies: a review. *J. Opt.* **47**, 307–317 (2018).
2. D Amico, I. et al. Nanoscale quantum optics. *RIV Nuovo Cimento* **42**, 153–195 (2019).
3. Aharonovich, I., Englund, D. & Toth, M. Solid-state single-photon emitters. *Nat. Photonics* **10**, 631–641 (2016).
4. Blatt, R. & Wineland, D. Entangled states of trapped atomic ions. *Nature* **453**, 1008–1015 (2008).
5. Shomroni, I. et al. All-optical routing of single photons by a one-atom switch controlled by a single photon. *Science* **345**, 903–906 (2014).
6. Firstenberg, O. et al. Attractive photons in a quantum nonlinear medium. *Nature* **502**, 71–75 (2013).
7. Nozaki, K. et al. Sub-femtojoule all-optical switching using a photonic-crystal nanocavity. *Nat. Photonics* **4**, 477–483 (2010).
8. Bradshaw, D. S., Forbes, K. A. & Andrews, D. L. Off-resonance control and all-optical switching: Expanded dimensions in nonlinear optics. *Appl. Sci.* **9**, 4252 (2019).
9. Hwang, J. et al. A single-molecule optical transistor. *Nature* **460**, 76–80 (2009).
10. Gurudev Dutt, M. V. et al. Quantum register based on individual electronic and nuclear spin qubits in diamond. *Science* **316**, 1312–1316 (2007).
11. Wei, H., Wang, Z., Tian, X., Käll, M. & Xu, H. Cascaded logic gates in nanophotonic plasmon networks. *Nat. Commun.* **2**, 387 (2011).
12. Ballarini, D. et al. All-optical polariton transistor. *Nat. Commun.* **4**, 1778 (2013).
13. Amo, A. et al. Exciton-polariton spin switches. *Nat. Photonics* **4**, 361–366 (2010).
14. Zasedatelev, A. V. et al. A room-temperature organic polariton transistor. *Nat. Photonics* **13**, 378–383 (2019).
15. Senellart, P., Solomon, G. & White, A. High-performance semiconductor quantum-dot single-photon sources. *Nat. Nanotechnol.* **12**, 1026–1039 (2017).
16. Somaschi, N. et al. Near-optimal single-photon sources in the solid state. *Nat. Photonics* **10**, 340–345 (2016).
17. Jin, C.-Y. & Wada, O. Photonic switching devices based on semiconductor nano-structures. *J. Phys. D* **47**, 133001 (2014).
18. Kim, H., Bose, R., Shen, T. C., Solomon, G. S. & Waks, E. A quantum logic gate between a solid-state quantum bit and a photon. *Nat. Photonics* **7**, 373–377 (2013).
19. He, Y.-M. et al. On-demand semiconductor single-photon source with near-unity indistinguishability. *Nat. Nanotechnol.* **8**, 213–217 (2013).
20. Pooley, M. A. et al. Controlled-not gate operating with single photons. *Appl. Phys. Lett.* **100**, 211103 (2012).
21. Volz, T. et al. Ultrafast all-optical switching by single photons. *Nat. Photonics* **6**, 605–609 (2012).
22. Wells, L. et al. Photon phase shift at the few-photon level and optical switching by a quantum dot in a microcavity. *Phys. Rev. Appl.* **11**, 061001 (2019).
23. Buterakos, D., Barnes, E. & Economou, S. E. Deterministic generation of all-photonic quantum repeaters from solid-state emitters. *Phys. Rev. X* **7**, 041023 (2017).
24. Javadi, A. et al. Spin-photon interface and spin-controlled photon switching in a nanobeam waveguide. *Nat. Nanotechnol.* **13**, 398–403 (2018).
25. Gea-Banacloche, J., Mumba, M. & Xiao, M. Optical switching in arrays of quantum dots with dipole-dipole interactions. *Phys. Rev. B* **74**, 165330 (2006).
26. Galland, C. et al. Dynamic hole blockade yields two-color quantum and classical light from dot-in-bulk nanocrystals. *Nano Lett.* **13**, 321–328 (2013).
27. Rivas, D. et al. Two-color single-photon emission from InAs quantum dots: toward logic information management using quantum light. *Nano Lett.* **14**, 456–463 (2014).
28. O'Brien, J. L., Furusawa, A. & Vučković, J. Photonic quantum technologies. *Nat. Photonics* **3**, 687–695 (2009).
29. Minzioni, P. et al. Roadmap on all-optical processing. *J. Opt.* **21**, 063001 (2019).
30. Johnsson, M. et al. Ultrafast carrier redistribution in single InAs quantum dots mediated by wetting-layer dynamics. *Phys. Rev. Appl.* **11**, 054043 (2019).
31. Gomis-Bresco, J. et al. Random population model to explain the recombination dynamics in single InAs/GaAs quantum dots under selective optical pumping. *New J. Phys.* **13**, 023022 (2011).
32. Ghosh, S. & Liew, T. C. H. Dynamical blockade in a single-mode bosonic system. *Phys. Rev. Lett.* **123**, 013602 (2019).
33. Jin, C.-Y. et al. Ultrafast non-local control of spontaneous emission. *Nat. Nanotechnol.* **9**, 886–890 (2014).
34. Benny, Y. et al. Excitation spectroscopy of single quantum dots at tunable positive, neutral, and negative charge states. *Phys. Rev. B* **86**, 085306 (2012).
35. Muñoz-Matutano, G. et al. Selective optical pumping of charged excitons in unintentionally doped inas quantum dots. *Nanotechnology* **19**, 145711 (2008).
36. Rudno-Rudziński, W. et al. Carrier diffusion as a measure of carrier/exciton transfer rate in inas/ingaasp/inp hybrid quantum dot-quantum well structures emitting at telecom spectral range. *Appl. Phys. Lett.* **112**, 051103 (2018).
37. Faraon, A., Majumdar, A., Kim, H., Petroff, P. & Vučković, J. Fast electrical control of a quantum dot strongly coupled to a photonic-crystal cavity. *Phys. Rev. Lett.* **104**, 047402 (2010).
38. Hallett, D. et al. Electrical control of nonlinear quantum optics in a nano-photonic waveguide. *Optica* **5**, 644–650 (2018).
39. Müller, M., Bounouar, S., Jöns, K. D., Glässl, M. & Michler, P. On-demand generation of indistinguishable polarization-entangled photon pairs. *Nat. Photonics* **8**, 224–228 (2014).
40. Muñoz-Matutano, G. et al. Size dependent carrier thermal escape and transfer in bimodally distributed self assembled InAs/GaAs quantum dots. *J. Appl. Phys.* **111**, 123522 (2012).
41. Miller, D. A. B. Are optical transistors the logical next step? *Nat. Photonics* **4**, 3–5 (2010).
42. Martín-Sánchez, J. et al. Single photon emission from site-controlled inas quantum dots grown on GaAs(001) patterned substrates. *ACS Nano* **3**, 1513–1517 (2009).
43. Gurioli, M., Wang, Z., Rastelli, A., Kuroda, T. & Sanguinetti, S. Droplet epitaxy of semiconductor nanostructures for quantum photonic devices. *Nat. Mater.* **18**, 799–810 (2019).
44. Srivastava, A. et al. Optically active quantum dots in monolayer WSe₂. *Nat. Nanotechnol.* **10**, 491–496 (2015).
45. Brotons-Gisbert, M. et al. Coulomb blockade in an atomically thin quantum dot coupled to a tunable fermi reservoir. *Nat. Nanotechnol.* **14**, 442–446 (2019).
46. Kremser, M. et al. Discrete interactions between a few interlayer excitons trapped at a MoSe₂ -WSe₂ heterointerface. Preprint at https://arxiv.org/abs/1907.08815 (2019).

47. Seravalli, L., Trevisi, G. & Frigeri, P. Design and growth of metamorphic InAs/InGaAs quantum dots for single photon emission in the telecom window. *CrystEngComm* **14**, 6833–6838 (2012).
48. Holmes, M. J., Choi, K., Kako, S., Arita, M. & Arakawa, Y. Room-temperature triggered single photon emission from a III-nitride site-controlled nanowire quantum dot. *Nano Lett.* **14**, 982–986 (2014).
49. Alén, B., Fuster, D., González, Y. & González, L. Tunable monolithic quantum light source and quantum circuit thereof. Patent application EP3361516A (2017).
50. Trevisi, G., Seravalli, L., Frigeri, P. & Franchi, S. Low density InAs/(In)GaAs quantum dots emitting at long wavelengths. *Nanotechnology* **20**, 415607 (2009).
51. Frigeri, P. et al. Effects of the quantum dot ripening in high-coverage InAs/GaAs nanostructures. *J. Appl. Phys.* **102**, 083506 (2007).

Acknowledgements

Author contributions

G.M.M. and D.R.G. carried out the spectroscopy and photon correlation experiments. G.M.M. built the experimental set-up. M.J., D.R.G., J.M.P. and G.M.M. implemented the master equation model and contributed to the analysis of the data. G.M.M. and M.J. have equally contributed to this research. L.S., G.T. and P.F. provided the quantum dot sample. G.M.M., M.G. and J.M.P. conceived the central idea of the work and related experiments, supervised the experimental work and M.J. and T.V. contributed to discussions. The manuscript was written by G.M.M. and M.J. with varying contributions from all other authors.

Competing interests

The authors declare no competing interests.

Additional information

Supplementary information is available for this paper at https://doi.org/10.1038/s42005-020-0292-8.

Correspondence and requests for materials should be addressed to G.M.-M.

Reprints and permission information is available at http://www.nature.com/reprints

Publisher's note Springer Nature remains neutral with regard to jurisdictional claims in published maps and institutional affiliations.